YBBRC 9714 ARTICLE IN PRESS No. of pages: 8
DISK / 30/8/03 / Bush(CE) / Anitha(TE) DTD 4.3.1 / SPS

Available online at www.sciencedirect.com

SCIENCE DIRECT®

ACADEMIC PRESS

BBRC

Biochemical and Biophysical Research Communications 309 (2003) 40–47

www.elsevier.com/locate/ybbrc

Mutagenesis study on the role of a lysine residue highly conserved in formate dehydrogenases and periplasmic nitrate reductases☆

Thomas Hettmann,[a] Roman A. Siddiqui,[a] Johannes von Langen,[a] Christa Frey,[a] Maria J. Romão,[b] and Stephan Diekmann[a,*]

[a] *Institute for Molecular Biotechnology, Beutenbergstr. 11, Jena DE-07745, Germany*
[b] *REQUIMTE, CQFB, Departamento de Química, FCT, Universidade Nova de Lisboa, Caparica 2829-516, Portugal*

Received 25 August 2003

Abstract

The lysine 85 (K85) in the primary structure of the catalytic subunit of the periplasmic nitrate reductase (NAP-A) of *Ralstonia eutropha* H16 is highly conserved in periplasmic nitrate reductases and in the structurally related catalytic subunit of the formate dehydrogenases of various bacterial species. It is located between an [4Fe–4S] center and one of the molybdopterin-guanine dinucleotides mediating the through bonds electron flow to convert the specific substrate of the respective enzymes. To examine the role of K85, the structure of NAP-A of *R. eutropha* strain H16 was modeled on the basis of the crystal structure from the *Desulfovibrio desulfuricans* enzyme (Dias et al. Structure Fold Des. 7(1) (1999) 65) and K85 was replaced by site-directed mutagenesis, yielding K85R and K85M, respectively. The specific nitrate reductase activity was determined in periplasmic extracts. The mutant enzyme carrying K85R showed 23% of the wild-type activity, whereas the replacement by a polar, uncharged residue (K85M) resulted in complete loss of the catalytic activity. The reduced nitrate reductase activity of K85R was not due to different quantities of the expressed gene product, as controlled immunologically by NAP-specific antibodies. The results indicate that the K85 is optimized for the electron transport flux to reduce nitrate to nitrite in NAP-A, and that the positive charge alone cannot meet further structural requirement for efficient electron flow.

Keywords: Nitrate reductase; Oxidoreductases; Electron transfer; FeS center; Molybdopterin; *Ralstonia eutropha*; *Desulfovibrio desulfuricans*

Many oxidoreductases contain transition metals at their active site. Molybdenum (Mo) and tungsten (W) are present in biological systems as part of the nitrogenase co-factor or bound to the organic co-factor pyranopterin. The molybdopterin or pyranopterin class of enzymes is diverse and has been subdivided into three main families [1]: the xanthine oxidase family, the sulfite oxidase family, and the DMSO reductase family. Within the variety of enzymes belonging to the DMSO reductase family, the periplasmic dissimilatory/respiratory nitrate reductases (NAP) as well as the formate dehydrogenases (FDH) share the highest degree of structural similarity in terms of their three-dimensional structures. So far, only one crystal structure of a periplasmic nitrate reductase has been solved (*D.d.* NAP, isolated from the sulfate reducer *Desulfovibrio* (*D.*) *desulfuricans* (*d.*) ATCC27774) [2,3], while three crystal structures are currently available for formate dehydrogenases: The FDH-H (part of the hydrogen lyase complex) from *Escherichia coli* [4], the membrane protein FDH-N (expressed when growing anaerobically on nitrate) from *E. coli* [5], and the W-containing *D. gigas* formate dehydrogenase (*Dg*W-FDH) [6,7].

While *D.d.*NAP and *E.coli* FDH-H are monomeric enzymes consisting of 723 and 715 amino acids (aa), respectively, the *Dg*W-FDH is a heterodimeric enzyme

☆ *Abbreviations:* BSA, bovine serum albumin; *D.*, Desulfovibrio; DMSOR, dimethyl sulfoxide reductase; FDH, formate dehydrogenase; FDH-H, formate dehydrogenase component of the formate-hydrogen lyase complex of *E. coli*; FDH-N, nitrate-dependent formate dehydrogenase of *E. coli* when growing anaerobically on nitrate; MES, 2-(*N*-Morpholino)ethanesulfonic acid; MGD, molybdopterin guanine dinucleotide; Moco, pyranopterin-ene-1,2-dithiolate cofactor or molybdopterin.

* Corresponding author. Fax: +49-3641-656225.
E-mail address: diekmann@imb-jena.de (S. Diekmann).

0006-291X/$ - see front matter © 2003 Elsevier Inc. All rights reserved.
doi:10.1016/j.bbrc.2003.08.114

with 977 aa (α-) and 214 aa (β-subunit), and the *E. coli* FDH-N forms a trimeric complex of three subunits of 982 aa (α-), 290 aa (β-), and 217 aa (γ-subunit), which associate as trimers along the membrane.

The structures of *D.d.*NAP and *E. coli* FDH-H are functionally related to the large catalytic α-subunit of *Dg*W-FDH and of *E. coli* FDH-N. These catalytic α-subunits carry the molybdopterin cofactor (W/Mo[$(MGD)_2$,-SH/-OH,-SeCys] and Mo[$(MGD)_2$,-OH,-Cys] for FDHs and NAPs, respectively) as well as one [4Fe–4S] cluster. Although differing in their molecular weights, their structures can be superimposed showing that their respective core structures are quite similar. The superposition of the large subunit of *Dg*W-FDH with NAP shows an r.m.s. deviation of 2.0 Å for 636 Cα atoms, while the comparison with *E. coli* FDH-H gives a corresponding r.m.s. deviation of 2.1 Å for 659 Cα atoms [7]. The structure of the α-subunit of the *E.coli* FDH-N is superimposable with that from *E. coli* FDH-H with an r.m.s. deviation of 1.9 Å for 599 Cα atoms [5]. The classification of these homologous proteins in terms of the topology is also similar and the overall structure can be subdivided into four domains, two of which correspond to non-contiguous stretches of the polypeptide chain. In the larger proteins *E.coli* FDH-N and *Dg*W-FDH, the additional residues of the catalytic α-subunit are essentially distributed over the molecular surface as insertions in the whole polypeptide.

The differences between both kinds of enzymes (NAP and FDH) that account for their different substrate specificities (reduction of nitrate to nitrite or conversion of formate into carbon dioxide) are localized essentially in the vicinity of the Mo active site as well as in the tunnel leading to it [3]. However, the electron transport pathway between the Mo active site and an external physiological electron acceptor (or donor) is rather conserved and it has been assumed that a conserved Lys residue mediates the electron transfer between one of the molybdopterin cofactors and the relatively exposed [4Fe–4S] cluster [4]. This conserved lysine residue is also found in prokaryotic assimilatory nitrate reductases (for an overview see [8]). Interestingly, sequence alignment studies show that the membrane-bound respiratory nitrate reductases (NAR) carry an arginine residue at the corresponding position (for reviews see [1,9]). The aim of this work is to analyze the requirement of this residue (K85) in NAP-A by single mutagenesis studies in comparison to an arginine replacement, as to whether the positive charge at that position is sufficient or whether further structural constraints make the lysine residue indespensible for the nitrate reductase activity in periplasmic nitrate reductases. *Ralstonia eutropha* was chosen for this study because the strain is much better amenable to genetic manipulation and its NAP-A is highly homologous to that from *D. desulfuricans*. *D.d.*NAP is the simplest member of the periplasmic nitrate reductases, since it contains only the catalytic subunit. In contrast, the nitrate reductase from *R. eutropha* is a heterodimer as found in all other periplasmic nitrate reductases analyzed so far. We therefore modeled only the α-subunit of NAP from *R. eutropha* (*R.eu.* NAP-A) based on the *D. desulfuricans* structure and then carried out the Lys85 mutation studies.

Materials and methods

Bacterial strains and plasmids. The genes for the periplasmatic nitrate reductase of *R. eutropha* are not part of the bacterial chromosome but located on the 450 kb megaplasmid pHG1 [10]. For our mutation studies we used strain HF210 [11], the megaplasmid-free derivative of the wild-type strain H16 (DSM 428, ATCC 17699), together with plasmids containing the complete *nap* cluster (pGE49, pCH332) [12]. A complete list of bacterial strains and plasmids used in this study is given in Table 1.

Media and growth conditions. *R. eutropha* strains were grown aerobically at 30 °C with 0.4% (w/v) fructose as carbon source and 0.2% ammonium chloride (w/v) as nitrogen source in 100 ml mineral medium as described in [12,13]. Strains of *E. coli* were grown at 37 °C in Luria–Bertani medium [14]. Solid media contained 1.8% (w/v) agar. Antibiotics were added as appropriate for *R. eutropha* (tetracycline, 12.5 μg/ml) and for *E. coli* (tetracycline, 12.5 μg/ml; ampicillin, 100 μg/ml). Cell growth was monitored by measuring the optical density at 600 nm.

Mutation and cloning protocol. The complete *nap* cluster with the genes *nap*E, *nap*D, *nap*A, *nap*B, and *nap*C (total length 5.8 kb) was recloned into the vector pBC SK + (Stratagene) and subsequently in pMCS5 (MoBiTec, Germany) for further use yielding in the vector pTH100.

All cloning steps were carried out in *E. coli* strain DH5α (Invitrogen). A small part of the *nap* cluster (1192 bp in length) was amplified by PCR (for primers used in this study, see Table 1) with *Taq* polymerase (Eppendorf, Germany). The plasmid pCH332 containing the whole *nap*EDABC cluster was used as template DNA. During the amplification, mutations were introduced at particular sites by PCR mutagenesis leading to the wanted single amino acids replacements (K85R and K85M). The sequence and position of the oligonucleotides are listed in Table 1. The changes in the lysine codon AAG (exchange to arginine codon CGC or methionine codon ATG) are underlined. The sequence of the oligonucleotide Bgl2-100-sense is located on the sense strand of the *nap*A gene (position 965–984) about 100 nucleotides upstream of an *Bgl*II restriction site (position 1065), while the sequence of the oligonucleotide *Eco*RI + 100-anti is located on the anti-sense strand of the *nap*A gene (position 2137–2156) about 100 bp downstream of an *Eco*RI restriction site (position 2051).

The PCR products were introduced by TA cloning into the vector pCR 2.1-TOPO (Invitrogen, USA) to yield the plasmids pTOPO-K85R and pTOPO-K85M. The obtained mutated sequence was verified by DNA sequencing (MWG, Germany). The inserts carrying the mutations were excised from the vector by the restriction endonucleases *Bgl*II and *Eco*RI and ligated into the vector pTH100 replacing the wild-type *Bgl*II/*Eco*RI segment of the complete *nap* cluster to yield the vectors pTH101 (exchange K85R) and pTH102 (exchange K85M). The correct arrangement of the gene was verified by restriction analysis. The mutated *nap* cluster was cut out of the vectors pTH101 and pTH102 by the restriction endonucleases *Sma*I and *Swa*I and this blunt-ended fragment was cloned into the broad host range vector pCM62 [15] resulting in pTH201 (exchange K85R) and pTH202 (exchange K85M). The vector pCM62 had been treated with *Xba*I and the sticky ends had been filled by Klenow polymerase to yield blunt ends, too. In the same manner the wild-type *nap* cluster was cut out of vector

Table 1
Bacterial strains, vectors, and oligonucleotides

Strain, plasmid or oligonucleotide	Relevant characteristics	Reference or source
R. eutropha		
H16	Nar+, Nas+, Nap+, pHG1+	DSM 428, ATCC 17699
HF210	Nar+, Nas+, Nap- pHG1-; derivative of H16	[11]
E. coli		
DH5α	F^- ϕ80d*lac*ZΔM15Δ(*lac*ZYA-*arg*F) U169 *deo*R *rec*A1 *end*A1 *hsd*R17(r_k^-, m_k^+) *pho*A *sup*E44 λ^- *thi*-1 *gyr*A96 *rel*A1	Invitrogen
S17-1	Tra+ *recA pro thi hsdR chr*::RP4-2	[29]
Plasmids		
pBC SK+	Cm^R *lacZ′* f1*ori* ColE1*ori*; T3 promoter, T7 promoter	Stratagene
pBluescript SK+	Ap^R *lacZ′* f1*ori* ColE1*ori*; T3 promoter, T7 promoter	Stratagene
pMCS5	Ap^R *lacZ′* f1*ori* pBR322*ori*; T7promoter	MoBiTec, Göttingen, Germany
pCR 2.1-TOPO	Ap^R Km^R *lacZ′* pUC*ori* f1*ori*; T7 promoter	Invitrogen
pCM62	Broad-host-range vector, Tc^R *lacZ′ traJ′* ColE1*ori ori*V *ori*T	[15]
pVK102	Km^R Tc^R Mob+ RP4*ori*	[30]
pGE49	16-kb *Hin*dIII fragment of megaplasmid pHG1 in pVK102	[12]
pCH332	6.0-kb *Eco*RV–*Cla*I fragment of pGE49 in pBluescript SK+	[12]
pNapBC	6.0-kb *Eco*RV–*Cla*I fragment of pGE49 in pBC SK+	This study
pTOPO-K85R	1.2-kb PCR-product K85R in pCR 2.1-TOPO	This study
pTOPO-K85M	1.2-kb PCR-product K85M in pCR 2.1-TOPO	This study
pTH100	6.0-kb *Eco*RV–*Xho*I fragment of pNapBC in pMCS5	This study
pTH101	986-bp *Bgl*II–*Eco*RI fragment of pTOPO-K85R in pTH100	This study
pTH102	986-bp *Bgl*II–*Eco*RI fragment of pTOPO-K85M in pTH100	This study
pTH200	6.1-kb *Swa*I–*Sma*I fragment of pTH100 in pCM62	This study
pTH201	6.1-kb *Swa*I–*Sma*I fragment of pTH101 in pCM62	This study
pTH202	6.1-kb *Swa*I–*Sma*I fragment of pTH102 in pCM62	This study
Oligonucleotides		
Bgl2-100-sense	5′-AC CTC ACC TGC CTC CAC CAG-3′; position 965–984	This study
*Eco*RI + 100-anti	5′-TGG GGT CGG CGT ACA GTT CG-3′; position 2156–2137	This study
K85R-sense	5′-G AAC TGC GTC CGC GGC TAC TTC CTG TCC-3′; position 1303–1330	This study
K85R-anti	5′-G GAA GTA GCC GCG GAC GCA GTT CAG GCC-3′; position 1325–1298	This study
K85M-sense	5′-AAC TGC GTC ATG GGC TAC TTC CTG TC-3′; position 1304–1329	This study
K85M-anti	5′-GAA GTA GCC CAT GAC GCA GTT CAG GC-3′; position 1324–1299	This study

pTH100 and cloned into vector pCM62 to yield vector pTH200. Only those plasmids were chosen (named pTH200, pTH201, and pTH202) where the *nap* cluster was in anti-sense orientation to the lac promoter of the vector pCM62.

The vector pCM62 can be replicated in *E. coli* as well as in *R. eutropha*. The vectors pTH200, pTH201, and pTH202 were transformed into the *E. coli* strain S17-1 and subsequently mobilized from *E. coli* strain S17-1 to *R. eutropha* strain HF210 according to [12].

The transconjugants of *R. eutropha* harboring either a *nap* cluster with mutation or a wild-type *nap* cluster on a plasmid were grown in 100 ml cultures and harvested in the stationary phase. Periplasmic fractions of *R. eutropha* were prepared as described in [16].

Nitrate activity assay. Enzyme activity was determined in the periplasmic extracts as well as in crude cell extracts with the microtiterplate assay described by Borcherding et al. [17] with the following modifications: all buffers were flushed with argon prior to use to lower the oxygen concentration in the solution. 1.5 mM of benzyl viologen instead of methyl viologen was used as electron donor. The enzymatic reaction was carried out in a closed tube at 37 °C instead of incubating in the open microtiterplate at room temperature. The reaction buffer was either 50 mM MES/NaOH for the pH values 5.5, 6.0, and 6.5 or 50 mM potassium phosphate buffer for the pH values 7.0, 7.5, and 8.0.

Protein assay. Protein concentrations were determined in an assay based on the Lowry method [18]. As protein standard for quantification, BSA in distilled water was used at concentrations from 100 to 500 μg/ml. The product of the color reaction was measured at 750 nm in a microtiter plate reader (Spectra Max 250, Molecular Devices, USA). Protein concentration of each sample was determined eightfold.

SDS–PAGE and Western blot. Denaturing polyacrylamide gel electrophoresis was performed according to Laemmli [19]. The acrylamide and bisacrylamide concentration in the separating gel was adjusted to 12% total concentration and 1% cross-linkage. Protein samples were diluted with the same volume gel loading buffer containing 2% (v/v) β-mercaptoethanol and 2% (w/v) SDS. Samples were heated for 15 min to 60 °C prior to loading the gel. 7.5 μl of "Precision Plus Protein standards, dual colour" (Bio-Rad, Germany) was used as molecular weight markers. After the electrophoresis, gels were stained with Coomassie brilliant blue R-250.

Gels used for Western blot analysis were not stained, but blotted on a PVDF membrane (Immobilon-P, Millipore) using a semi-dry blot apparatus (Fast Blot B-33, Biometra, Göttingen, Germany). Blotting buffer consisted of 192 mM Glycin, 25 mM Tris, 1.3 mM SDS, and 20% (v/v) methanol. The gel was blotted for one hour at 4 mA/cm^2. After blotting the gel was stained with Coomassie brilliant blue R-250 to

check the completeness of the transfer. The PVDF membrane was blocked for 1 h with 5% skimmed milk powder in PBS–Tween (100 mM sodium phosphate buffer, pH 7.5, 100 mM NaCl, and 0.1% (w/v) Tween 20). The nitrate reductase was detected by a two-step incubation with antibodies, at first with an antiserum from rabbit against purified nirate reductase [16] diluted 1:1000 in PBS–Tween, second with goat-anti-rabbit IgG conjugated with peroxidase (Dianova, Hamburg, Germany) diluted 1:1000 in PBS–Tween. The color reaction was performed with a solution of a few crystals of 3,3′-diamino-benzidine dissolved in 10 ml of 50 mM sodium acetate, pH 5.0, containing 0.03% H_2O_2. The relative intensity of the NAP-A bands on the blot was determined using the MacCAM 1.0b (Cybertech) software.

Modeling the Ralstonia nitrate reductase structure. Based on the *D. desulfuricans* nitrate reductase [2], a three-dimensional model of NAP-A of *R. eutropha* nitrate reductase was constructed. First, a BLAST search was performed using the sequence of *R. eutropha*. Next, the amino acid sequence of the two nitrate reductases from *R. eutropha* (Swiss-Prot Accession No. P39185) and *D. sulfuricans* (P81186) as well as a third one from *E. coli* (P33937), and two sequences of two different formate dehydrogenases from *E. coli* (FDH-N, P24183; FDH-H, P07658) were aligned using the program ClustalX [20] applying the GONNET matrix [21]. Subsequently, corresponding amino acids in the *D. desulfuricans* structure were replaced by the *R. eutropha*-specific amino acids using the program MODELLER4.0 [22]. Finally, using the program PROCHECK [23], the obtained Phi and Psi angles of the backbone linkages were analyzed for unusual conformations by using a Ramachandran plot. These unusual conformations were corrected and modified towards more frequent structural arrangements. In addition, energetically unfavorable amino acids positions were optimized using the AMBER 6 software [24].

The alignment between the two amino acid sequences of *R.eu.*-NAP-A and *D.d.*NAP-A (Fig. 1A) was done using the ClustalW program [25] at the web page of NPS@ [26].

Results and discussion

Structural model of R. eutropha NAP-A

As the structural basis for our mutagenesis studies, we constructed a three-dimensional model of the catalytic subunit NAP-A from *R. eutropha* (*R.eu.*NAP-A) based on the *D. desulfuricans* structure (*D.d.*NAP). The *D. desulfuricans* nitrate reductase structure (1.9 Å resolution [2]) shows an amino acid identity of 37.5% with *R.eu.*NAP-A (see Fig. 1A). In order to find the structurally conserved regions within the oxidoreductase family, a BLAST search was performed using the *R.eu.*NAP-A primary structure. Next, the primary structure of several periplasmic nitrate reductases as well as two formate dehydrogenases was aligned (see Materials and methods for list of the proteins). This comparison identified the conserved regions of *R.eu.*NAP-A, as well as two additional loops of 25 and 43 amino acids (aa) in length, present only in *R.eu.*NAP-A (aa position 297–328 and 577–651; see Fig. 1B). Due to the lack of any homologous structure information and the length of those loop regions, we did not address any three-dimensional structure to these two loop segments by modeling, as their significance would be poor.

Subsequently, we replaced the corresponding amino acids in the *D. desulfuricans* structure by the varying *R. eutropha* amino acids and super-positioned the backbone atoms by using spatial restraints. In this way, an energetically favorable structure for the deletions and insertions was calculated. The amino acid side chains of the conserved residues were oriented according to the rotamer positions in the crystal structure; the remaining rotamers of the differing residues were modeled. Unusual conformations were corrected and modified towards arrangements found more frequently in other structures. In addition, energetically unfavorable amino acids positions were optimized.

We noticed that the major sequence differences between the two structures, the two loops in the *Ralstonia* enzyme, are not related to the essential structural elements linked to electron transport, pterin positioning or the active site, but are located at the protein surface. The functionally relevant protein parts required for catalytic nitrate reduction as compared to the *D.d.*NAP remain nearly unmodified (see Fig. 1B).

Mutant analysis

The genes for the periplasmatic nitrate reductase of *R. eutropha* strain H16 are not part of the bacterial chromosome but located on a megaplasmid. We introduced the desired mutations into the *napA* gene by site-directed mutagenesis and used a periplasmic nitrate reductase negative and megaplasmid-free derivative of the wild-type H16, *R. eutropha* HF210 as the host to study the effect of the mutant enzymes.

The four strains studied (wild-type *nap*EDABC, mutant K85R, mutant K85M, and *nap*-negative strain HF210) were grown in 100 ml cultures in at least three independent experiments, harvested in the stationary phase, and the periplasm was isolated.

Nitrate reductase activity was determined in whole cell and in periplasmic extracts but not in further purified form to avoid loss of activity during the four-step purification procedure (including ammonium sulfate precipitation, hydrophobic interaction and cation exchange chromatography, and gel filtration [12]) and to keep the enzyme in a "as native as possible" state.

The activity assay was carried out with benzyl viologen (BV) as artificial electron donor. It is not clear if BV transfers the electrons first to the heme groups of NapB and then via the [4Fe–4S] cluster of NapA to the Mo center as the physiological electron donor (NapC) does. Alternatively, BV might transfer electrons directly to the [4Fe–4S] cluster. In all cases, Lys85 is part of the electron transfer path. Direct electron transfer to the Mo center by BV is highly improbable as the Mo center is deeply buried in the NapA protein (see Fig. 1B) and is accessible only via the cavity through which nitrate enters the active center.

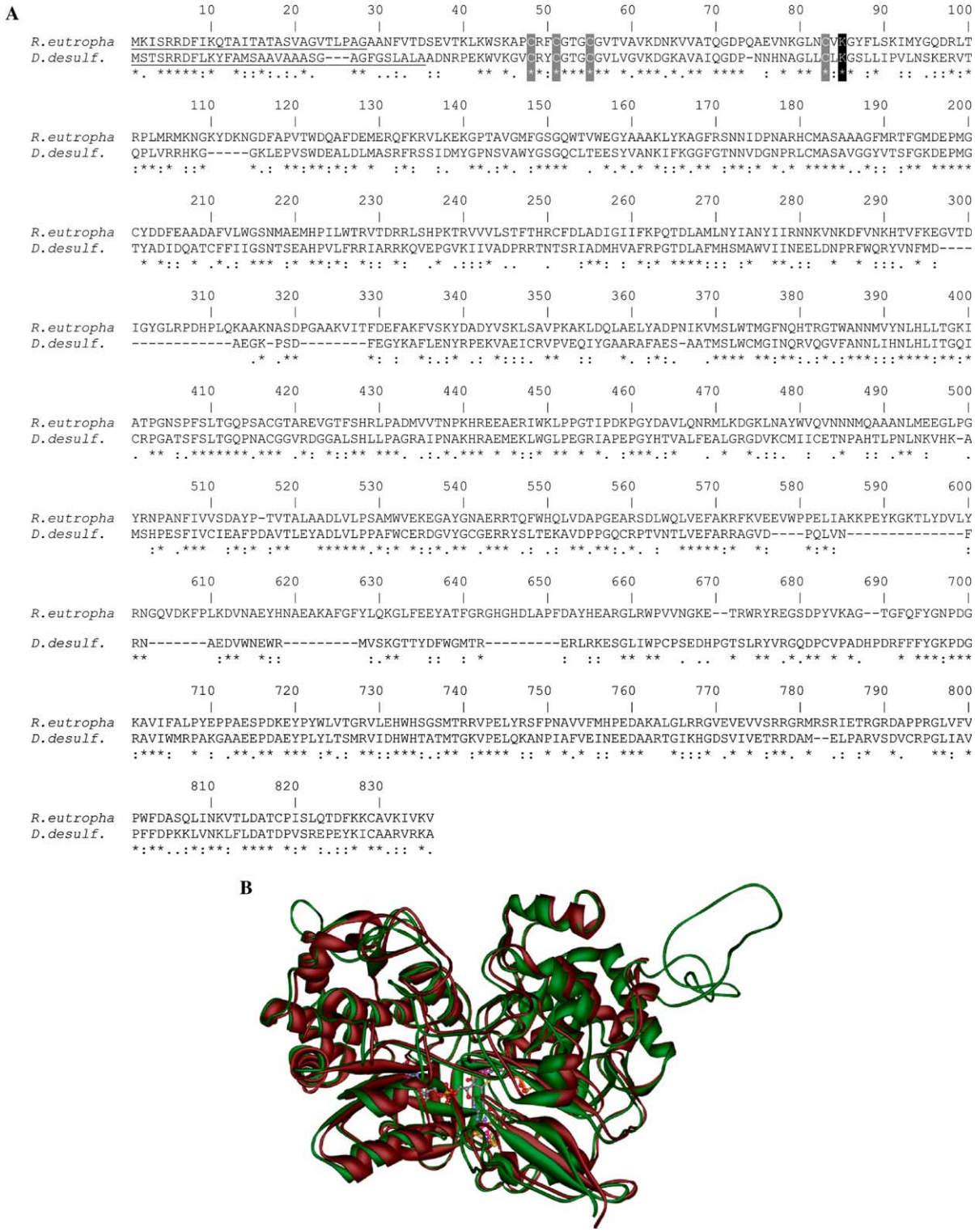

Fig. 1. (A) Homology comparison of the amino acid sequences of the *D. desulfovibrio* and the *R. eutropha* nitrate reductase catalytic subunit NAP-A. The signal peptides are underlined. Identical amino acids are marked by asterisks (*), strongly similar amino acids are marked by two dots (:), weakly similar amino acids are marked by one dot (.). The four conserved cysteine residues binding the [4Fe–4S] cluster are highlighted by white font on grey background; the lysine 85 is highlighted by white font on black background. (B) Structural superimposition of the catalytic subunits NAP-A of the periplasmic nitrate reductases from *D. desulfovibrio* (dark red) and *R. eutropha* (green). (For interpretation of the references to color in this figure legend, the reader is referred to the web version of this paper.)

The pH-dependent activity of the wild-type nitrate reductase was examined in the pH range from pH 5.5 to 8.0. Maximum activity was found at pH 6.5 (data not shown); thus, the subsequent activity assays for the NAP mutants were carried out at pH 6.5.

The strain containing the wild-type *nap*EDABC exhibited specific nitrate reductase activities between 0.522 and 0.987 U/mg at pH 6.5 with an average of 0.73 U/mg (see Table 2). One activity unit U is defined as 1 μmol nitrite formed per minute at 37 °C and at pH 6.5. The strain with the amino acid exchange K85R showed activity values between 0.090 and 0.251 U/mg with an average of 0.17 U/mg (four independent experiments). This corresponds to an activity of the K85R mutant relative to the wild-type of $(23 \pm 10)\%$ (comparison of the mean values). The strain carrying the *nap* cluster with the mutation K85M showed no nitrate reductase activity (three independent experiments), neither did the *nap*-negative strain HF210 which served as a negative control (three independent experiments).

This discrepancy in specific activity is not due to different amounts of nitrate reductase produced by the different mutants. To verify this, the amount of nitrate reductase was checked by Western blot analysis (see Fig. 3). As expected, neither NAP-A nor NAP-B protein can be detected in the *nap*-negative strain HF210 (negative control, lane 1). Only a few very faint bands of proteins cross-reacting with the antiserum against the periplasmic nitrate reductase of *R. eutropha* can be detected. Lane 2 (wild-type), 3 (mutant K85R), and 4 (mutant K85M) show similar intensities for the catalytic α-subunit (NAP-A) and for the smaller β-subunit (NAP-B): The intensity of the NAP-A-bands was determined by applying a gel analysis program and was found to be 36.5 arbitrary area units for the wild-type, 37.6 area units for K85R, and 26.7 area units for K85M. Within the error, both strains showing nitrate reductase activity, i.e., wild-type and the K85R mutant, have the same NAP-A band intensity and thus the same amounts of enzyme in the periplasmic extract analyzed.

In addition to the examination of the periplasmic fractions, the nitrate reductase activity was also studied in crude extracts of whole cells obtained by sonification of *R. eutropha* cells. This was done for all 4 strains examined above: the wild-type nitrate reductase as well as the two mutants, and—as control—the *nap*-negative strain. Also in this case, the expression levels of the nitrate reductase were studied by Western blot analysis. The nitrate reductase activity results from these whole cell extract experiments (data not shown) are in complete agreement with the results obtained with samples from the periplasmic fractions.

The conserved positively charged Lys residue shows optimal nitrate reductase activity in contrast to the mutant with the K85M replacement that exhibits no nitrate reductase activity. However, the positively charged mutant K85R still shows 23% activity relative to wild-type. These results indicate that a positive charge is required at this protein site for nitrate reductase activity. In all related crystal structures, the electron transfer from the Mo site to an external electron acceptor/donor involves the [4Fe–4S] center and is mediated by a Lys residue, strongly conserved in all periplasmic nitrate reductases as well as in formate dehydrogenases. This Lys is located two residues after the fourth Cys ligand of the [4Fe–4S] cluster with the conserved motif:

C-XX-C-XX-GC——CXK^{85}G

As depicted in Fig. 2, the conserved Lys makes a hydrogen bond with the exocyclic NH_2 group of the pterin. The contact to the [4Fe–4S] center is through an NH—S bond involving the NH_2^{ζ} group of the same Lys and the S^{γ}-Cys^{n-2}, a ligand of the [4Fe–4S] center. The importance of the conserved Lys is, at first instance, to create a favorable through bond electron transfer pathway between the two metal centers which are at a distance (Mo—nearest Fe is 12.6 Å for *D.d.*NAP) [27] that allows efficient electron tunneling. Interestingly, in all molybdopterin enzymes of the Xanthine Oxidase family [28] electron transfer between the redox centers (molybdopterin and $2 \times$[2Fe–2S]) involves the (direct) contact (NH–S bond) of the pterin-NH_2 to the S^{γ} of one of the cysteines of the nearest [2Fe–2S] cluster, but without the mediation of an amino-acid side chain.

Alignment of the amino acid sequences from formate dehydrogenases (FDH), periplasmic nitrate reductases (NAP), and respiratory membrane-bound nitrate re-

Table 2
Specific nitrate reductase activity of wild-type, K85M, K85R, and HF210

Strain	Specific activity in different independent experiments (U/mg)				Average activity (U/mg)	Percentile activity
	1	2	3	4		
Wild-type NAP	0.522	0.859	0.987	0.563	0.73	≡ 100%
Mutant K85R	0.251	0.207	0.090	0.142	0.17	23%
Mutant K85M	0	0	0	—	0	0%
nap-Negative strain (HF210)	0	0	0	—	0	0%

The different strains were grown in three to four independent experiments, periplasma was prepared, and the specific nitrate reductase activity in the periplasm was determined.

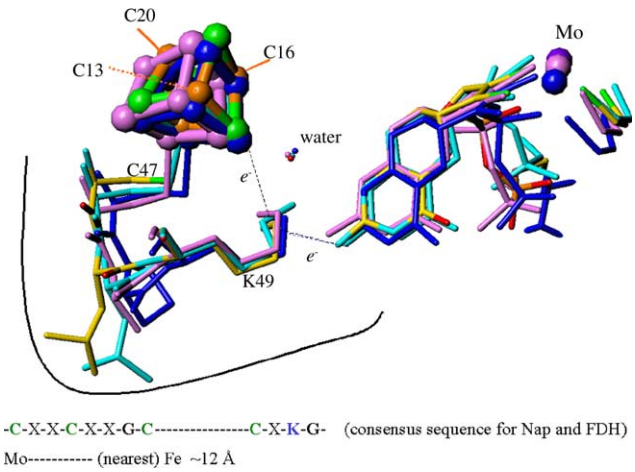

Fig. 2. Super positioning of the bis-MGD cofactor (including the Mo/W atom and its ligands, OH/SH and Cys/SeCys), the [4Fe–4S] cofactor and the conserved Lys, which mediates the electron transfer to an external electron acceptor. Residues numbering correspond to *D.d.*NAP. The *D.d.*NAP is represented in color code, the *E. coli* FDH-H in light blue, the *D. gigas* W-FDH in pink, and *E. coli* FDH-N in dark blue. Only crystal structures are displayed. Our modeled structure is not presented; it would super-impose the *D. desulfuricans* NAP. The distances between the NH_2^{ζ} group of the conserved Lys and the pterin-NH_2 vary between 3.01 and 3.12 Å in *D.d.*NAP, FDH-H, W-FDH, and FDH-N. The contact between the Lys and the [4Fe–4S] is established by NH—S bonds with the S^{γ}-Cys of the cluster. (For interpretation of the references to color in this figure legend, the reader is referred to the web version of this article.)

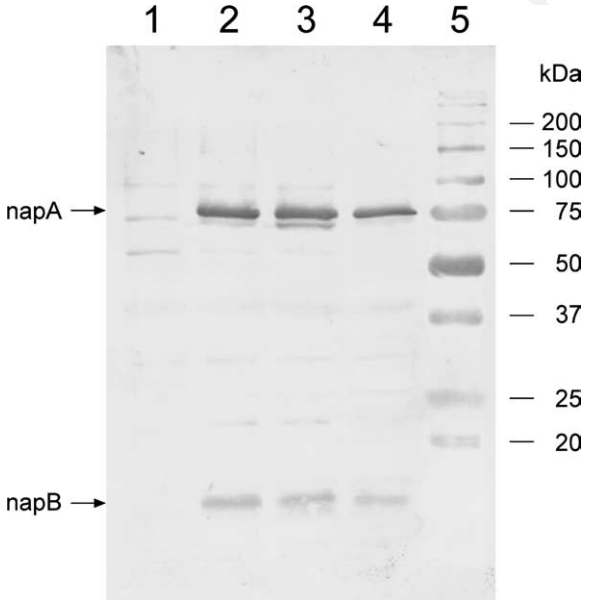

Fig. 3. Western blot analysis of periplasmic extracts from different *Ralstonia eutropha* strains. Lanes 1–4 each contain 15 μg of periplasmic protein. Lane 1—*nap* -negative, megaplasmid-free strain HF210; lane 2—strain HF210 harboring plasmid pTH200 (containing the wild-type *nap*EDABC cluster); lane 3—strain HF210 harboring plasmid pTH201 (like pTH200 but with single amino acid exchange K85R); lane 4—strain HF210 harboring plasmid pTH202 (like pTH200 but with single amino acid exchange K85M); and lane 5—molecular weight standard (7.5 μl Precision Plus Protein standard, dual colour, Bio-Rad).

ductases (NAR) shows that the latter enzymes carry a conserved arginine at the position corresponding to K85 of *R. eutropha* NAP-A (see reviews [1,9]). Also in the light of our results, it seems very probable that in respiratory nitrate reductases this conserved Arg residue mediates electron transfer from the [4Fe–4S] center to Moco in a similar way as the Lys residue does in NAP and FDH. Until now, no crystal structure of a respiratory nitrate reductase (NAR) has been solved. Hence, the exact three-dimensional arrangement of the [4Fe–4S] center, MoCo and the Arg side chain in NAR is not known. However, due to the sequence homologies one might anticipate similarities of the three-dimensional structure of NAR with NAP and FDH, at least in regions important for catalysis. Nevertheless, the two consensus sequences of NAR on the one hand and NAP and FDH on the other hand differ at least in one aspect: the first ligand of the [4Fe–4S] center is a His in NAR and a Cys in NAP and FDH:

C-X-X-**C**-X-X-G-**C**——**C**-X-**K**-G (consensus sequence for NAP and FDH)

H-X-X-X-**C**-X-X-X-**C**——**C**-P-**R**-G (consensus sequence for NAR)

Obviously, R is tolerated instead of K at position 85. It is thus not really surprising that the mutant K85R shows activity. Based on the similarities between the two groups of enzymes, we might expect that the exchange K85R would cause only a minor decrease in enzyme activity. Instead, the observed decrease in activity of $(77 \pm 10)\%$ for the K85R mutant—although also carrying a positive charge—can be tentatively explained by considering the larger size of the Arg side chain, which may change the framework of the through bond electron transfer pathway rendering it somewhat less effective. Although the general three-dimensional arrangements of the [4Fe–4S] center and the MoCo can be speculated to be similar in NAR and NAP, this through-bond electron transfer pathway might differ between these two groups of enzymes. Alternatively, the function of the Arg might be coupled to the presence of the His ligand of the iron–sulfur center. Following this line of arguments, full activity would only be expected for the combinations C-C-C-C-K (NAP, FDH) and H-C-C-C-R (NAR), but not for mixtures like C-C-C-C-R (mutation K85R) or H-C-C-C-K. Future mutagenesis studies will elucidate this point.

In the case of the K85M, the electron tunneling will probably be disturbed, since no hydrogen bonds can be established between the pterin moiety and the [4Fe–4S] cluster. In addition, the absence of a positive charge will certainly imply changes in the relative redox potentials of the metal centers. The effect will be probably higher in the nearest Fe/S center than in the Mo site with a consequent decrease in its redox potential.

The efficient electron transport in periplasmic nitrate reductases seems to require a positively charged residue

placed between the cofactors: (1) to modulate the redox potential of the involved metal sites and (2) to create a through-bond electron transfer path between the redox centers. These conclusions should however be regarded as tentative and a more detailed study will require the production of the pure mutants, a more detailed enzymological study on the purified proteins, and the determination of the respective crystal structures, which is planned for the near future.

Acknowledgments

We thank the DFG for funding our work (SFB 436, project B7). We thank P. Steinrücke and C. Cunha for many helpful discussions and J.M. Dias for help with the figures. M.J.R. thanks the Alexander von Humboldt Foundation for a follow-up fellowship.

References

[1] R. Hille, The mononuclear molybdenum enzymes, Chem. Rev. 96 (7) (1996) 2757–2816.
[2] J.M. Dias, M.E. Than, A. Humm, R. Huber, G.P. Bourenkov, H.D. Bartunik, S. Bursakov, J. Calvete, J. Caldeira, C. Carneiro, J.J. Moura, I. Moura, M.J. Romão, Crystal structure of the first dissimilatory nitrate reductase at 1.9 Å solved by MAD methods, Structure Fold Des. 7 (1) (1999) 65–79.
[3] M.J. Romão, J.M. Dias, I. Moura, Dissimilatory nitrate reductase (NAP), in: K. Wieghardt, R. Huber, T.L. Poulos, A. Messerschmidt (Eds.), Handbook of Metalloproteins, Wiley-VCH, 2001, pp. 1075–1085.
[4] J.C. Boyington, V.N. Gladyshev, S.V. Khangulov, T.C. Stadtman, P.D. Sun, Crystal structure of formate dehydrogenase H: catalysis involving Mo, molybdopterin, selenocysteine, and an Fe4S4 cluster, Science 275 (5304) (1997) 1305–1308.
[5] M. Jormakka, S. Tornroth, B. Byrne, S. Iwata, Molecular basis of proton motive force generation: structure of formate dehydrogenase-N, Science 295 (5561) (2002) 1863–1868.
[6] H. Raaijmakers, S. Teixeira, J.M. Dias, M.J. Almendra, C.D. Brondino, I. Moura, J.J. Moura, M.J. Romão, Tungsten-containing formate dehydrogenase from *Desulfovibrio gigas*: metal identification and preliminary structural data by multi-wavelength crystallography, J. Biol. Inorg. Chem. 6 (4) (2001) 398–404.
[7] H. Raaijmakers, S. Macieira, J. Dias, S. Teixeira, S. Bursakov, R. Huber, J. Moura, I. Moura, M. Romão, Gene sequence and the 1.8 Å crystal structure of the tungsten- containing formate dehydrogenase from *Desulfovibrio gigas*, Structure (Camb.) 10 (9) (2002) 1261.
[8] D.J. Richardson, B.C. Berks, D.A. Russell, S. Spiro, C.J. Taylor, Functional biochemical and genetic diversity of prokaryotic nitrate reductases, Cell. Mol. Life Sci. 58 (2) (2001) 165–178.
[9] L. Philippot, O. Højberg, Dissimilatory nitrate reductases in bacteria, Biochim. Biophys. Acta 1446 (1–2) (1999) 1–23.
[10] U. Warnecke-Eberz, B. Friedrich, Three nitrate reductase activities in *Alcaligenes eutrophus*, Arch. Microbiol. 159 (1993) 405–409.
[11] C. Kortlüke, K. Horstmann, E. Schwartz, M. Rohde, R. Binsack, B. Friedrich, A gene complex coding for the membrane-bound hydrogenase of *Alcaligenes eutrophus* H16, J. Bacteriol. 174 (19) (1992) 6277–6289.
[12] R.A. Siddiqui, U. Warnecke-Eberz, A. Hengsberger, B. Schneider, S. Kostka, B. Friedrich, Structure and function of a periplasmic nitrate reductase in *Alcaligenes eutrophus* H16, J. Bacteriol. 175 (18) (1993) 5867–5876.
[13] H.G. Schlegel, H. Kaltwasser, G. Gottschalk, Ein Submersverfahren zur Kultur wasserstoffoxidierender Bakterien: wachstumsphysiologische Untersuchungen, Arch. Mikrobiol. 38 (1961) 209–222.
[14] S. Sambrook, E.F. Fritsch, T. Maniatis, Molecular Cloning: A Laboratory Manual, second ed., Cold Spring Harbor Laboratory, Cold Spring Harbor, NY, 1989.
[15] C.J. Marx, M.E. Lidstrom, Development of improved versatile broad-host-range vectors for use in methylotrophs and other Gram-negative bacteria, Microbiology 147 (2001) 2065–2075.
[16] M. Bernhard, B. Friedrich, R.A. Siddiqui, *Ralstonia eutropha* TF93 is blocked in tat-mediated protein export, J. Bacteriol. 182 (3) (2000) 581–588.
[17] H. Borcherding, S. Leikefeld, C. Frey, S. Diekmann, P. Steinrücke, Enzymatic microtiter plate-based nitrate detection in environmental and medical analysis, Anal. Biochem. 282 (1) (2000) 1–9.
[18] O.H. Lowry, N.J. Rosebrough, A.L. Farr, R.J. Randall, Protein measurement with the folin phenol reagent, J. Biol. Chem. 193 (1951) 265–275.
[19] U.K. Laemmli, Cleavage of structural proteins during the assembly of the head of Bacteriophage T4, Nature 227 (1970) 680–685.
[20] J.D. Thompson, T.J. Gibson, F. Plewniak, F. Jeanmougin, D.G. Higgins, The CLUSTAL_Xwindows interface: flexible strategies for multiple sequence alignment aided by quality analysis tools, Nucleic Acids Res. 25 (24) (1997) 4876–4882.
[21] R. Baeza-Yates, G.H. Gonnet, A new approach to text searching, Commun. ACM 35 (10) (1992) 74–82.
[22] A. Sali, T.L. Blundell, Comparative protein modelling by satisfaction of spatial restraints, J. Mol. Biol. 234 (3) (1993) 779–815.
[23] R.A. Laskowski, M.W. MacArthur, D.S. Moss, J.M. Thornton, PROCHECK: a program to check the stereochemical quality of protein structures, J. Appl. Cryst. 26 (1993) 283–291.
[24] D.A. Case, D.A. Pearlman, J.W. Caldwell, T.E.I. Cheatham, W.S. Ross, C.L. Simmerling, T.A.D.K.M. Merz, R.V. Stanton, A.L. Cheng, J.J. Vincent, M. Crowley, V. Tsui, R.J. Radmer, Y. Duan, J. Pitera, I. Massova, G.L. Seibel, U.C. Singh, P.K. Weiner, P.A. Kollman, AMBER 6, University of California, San Francisco, 1999.
[25] J.D. Thompson, D.G. Higgins, T.J. Gibson, CLUSTAL W: improving the sensitivity of progressive multiple sequence alignment through sequence weighting, position-specific gap penalties and weight matrix choice, Nucleic Acids Res. 22 (22) (1994) 4673–4680.
[26] C. Combet, C. Blanchet, C. Geourjon, G. Deleage, NPS@: network protein sequence analysis, Trends Biochem. Sci. 25 (3) (2000) 147–150.
[27] C.C. Page, C.C. Moser, X. Chen, P.L. Dutton, Natural engineering principles of electron tunnelling in biological oxidation–reduction, Nature 402 (6757) (1999) 47–52.
[28] M.J. Romão, J. Knäblein, R. Huber, J.J. Moura, Structure and function of molybdopterin containing enzymes, Prog. Biophys. Mol. Biol. 68 (2–3) (1997) 121–144.
[29] R. Simon, U. Priefer, A. Pühler, A broad host range mobilization system for in vivo genetic engineering: transposon mutagenesis in Gram-negative bacteria, Biotechnology 1 (1983) 784–791.
[30] V.C. Knauf, E.W. Nester, Wide host range cloning vectors: a cosmid clone bank of an Agrobacterium Ti plasmid, Plasmid 8 (1) (1982) 45–54.